Atmospheric Science Faculty Publications   Atmospheric Science

5-1-2012

Single Aircraft Integration of Remote Sensing and In Situ Sampling for the Study of Cloud Microphysics and Dynamics

Zhien Wang
University of Wyoming

Jeffrey French
University of Wyoming, jfrench@uwyo.edu

Gabor Vali
University of Wyoming, vali@uwyo.edu

Perry Wechsler
University of Wyoming, wex@uwyo.edu

Samuel Haimov
University of Wyoming, haimov@uwyo.edu

See next page for additional authors

Follow this and additional works at: http://repository.uwyo.edu/atmospheric_facpub

Part of the Engineering Commons

Authors

Zhien Wang, Jeffrey French, Gabor Vali, Perry Wechsler, Samuel Haimov, Alfred Rodi, Min Deng, Dave Leon, Jeff Snider, Liran Peng, and Andrew L. Pazmany

SINGLE AIRCRAFT INTEGRATION OF REMOTE SENSING AND IN SITU SAMPLING FOR THE STUDY OF CLOUD MICROPHYSICS AND DYNAMICS

by Zhien Wang, Jeffrey French, Gabor Vali, Perry Wechsler, Samuel Haimov, Alfred Rodi, Min Deng, Dave Leon, Jeff Snider, Liran Peng, and Andrew L. Pazmany

Radar, radiometer, lidar, and in situ sensors working together aboard the University of Wyoming's King Air yield more complete descriptions of clouds than possible when combining ground-based remote sensing with airborne in situ measurements.

Poor understanding of cloud–radiation–dynamics feedbacks results in large uncertainties in forecasting human-induced climate changes (Soden and Held 2006; Solomon et al. 2007). Improving our understanding of cloud physics based on observational data is a critical step to improve physically based cloud microphysics

AFFILIATIONS: Wang, French, Vali, Wechsler, Haimov, Rodi, Deng, Leon, Snider, and Peng—Department of Atmospheric Science, University of Wyoming, Laramie, Wyoming; Pazmany—ProSensing, Inc., Amherst, Massachusetts
CORRESPONDING AUTHOR: Zhien Wang, Department of Atmospheric Science, University of Wyoming, Dept. 3038, 1000E University Ave. Laramie, WY 82071
E-mail: zwang@uwyo.edu

The abstract for this article can be found in this issue, following the table of contents.

parameterizations for climate and weather models (NRC 1998; Randall et al. 2003; Stoelinga et al. 2003; Fritsch and Carbone 2004; Klein et al. 2009). Airborne in situ cloud observations have played an important role in advancing our understanding of cloud microphysical and dynamic processes by providing detailed measurements at high temporal and spatial resolution (Rangno and Hobbs 1991 and 2001; Heymsfield and Miloshevich 1993; Stevens et al. 2003; Baker and Lawson 2006; McFarquhar et al. 2007; Bailey and Hallett 2009). However, these detailed measurements are only available along a line defined by the flight path of the aircraft. Interpretation of hydrometeor measurements from in situ probes is further limited because of their small sample volumes ranging from ~1 to ~10^5 cm^3 s^{-1}. The small sampling volume, particularly for ice crystals and drizzle drops, is an issue when one wishes to study atmospheric properties with strong spatial inhomogeneity or low concentration (Isaac and Schmidt 2009).

Airborne remote sensing overcomes these weaknesses of in situ sampling; however, the measurements

reflect integrated cloud properties, not the size-resolved distributions of in situ sampling. In addition to measures of hydrometeor properties, airborne radars provide unique measurements of cloud-, precipitation-, and cloud-scale dynamics (Hildebrand et al. 1996; Heymsfield et al. 1996; Vali et al. 1998; Stevens et al. 2003; Damiani et al. 2006; Leon et al. 2006). Lidars operate at much shorter wavelengths than radars and have capabilities to measure aerosols and optically thin clouds (McGill et al. 2002; Wang et al. 2009). Because these two types of active remote sensors, plus radiometers, have different sensitivities to particles of different size, it is possible to optimally combine multiple remote sensor measurements in cloud macrophysical and microphysical property retrievals (Wang and Sassen 2001, 2002; Stephens et al. 2002).

Integration of the complementary capabilities of airborne in situ sampling and remote sensing has great advantages for the study of atmospheric processes. For example, 2D cross sections of cloud microphysical properties retrieved from remote sensor measurements provide a context to understand

detailed in situ cloud measurements. The integration of in situ and remote sensing can be achieved with one or more aircrafts in a field campaign. The National Aeronautics and Space Administration (NASA) Cirrus Regional Study of Tropical Anvils and Cirrus Layers–Florida-Area Cirrus Experiment (CRYSTAL-FACE; www.espo.nasa.gov/crystalface /index.html) in 2002 is a great example of multiple-aircraft remote sensing and in situ sampling integration. However, even with carefully coordinated multiple aircraft flights, CRYSTAL-FACE data demonstrated the difficulty in acquiring spatially and temporally collocated data (Wang et al. 2005) with multiple aircraft.

Airborne research at the University of Wyoming began nearly 50 years ago. Since the mid-1960s, researchers at the university have utilized three different aircraft to acquire measurements throughout the lower troposphere (Rodi 2011). The University of Wyoming King Air (UWKA), the most current aircraft, is a specially modified Beechcraft Super King Air 200T for research in the lower to midtroposphere, including cloud physics studies. It was originally

TABLE 1. A list of major cloud physics and aerosol instrumentation on the UWKA.	
Instrument	**Capability**
Remote sensing	
WCR	Z_e and Doppler velocity
WCL	Backscattering coefficient and linear depolarization ratio
GVR	LWP and total PWV
In situ sampling (hydrometeor)	
DMT CDP	Cloud droplet size spectra within 2–50 μm (30 channels)
PMS FSSP	Cloud droplet size spectra [15 channels with lower and upper limits typically set at 1.5 and 47.5 μm; Vali et al. (1998)]
PMS OAP-2DC	Two-dimensional particle images [20 channels with lower and upper limits set at 25 and 7,000 μm, respectively; Gordon and Marwitz (1984)]
Fast OAP-2DC grayscale with 64 diodes	Two-dimensional particle images (100 channels with bin boundaries starting at 13 μm and extending to 2,513 μm in 25-μm increments)
PMS OAP-2DP	Two-dimensional particle images [20 channels with lower and upper limits set at 100 and 10,000 μm, respectively; Gordon and Marwitz (1984)]
Gerber PVM 100A	Cloud liquid water content from droplets up to ~60 μm
DMT LWC100 (hotwire)	Cloud liquid water content from droplets up to ~50 μm
Rosemount ice detector	Super-cooled liquid water content/icing rate
In situ sampling (aerosol)	
TSI CPC3010 (CN counter)	Aerosol particle concentrations larger than 15 nm
TSI CPC3025	Aerosol particle concentrations larger than 3 nm
DMT PCASP with SPP200	Aerosol size spectra [30 channels with upper and lower limits set at 0.1 and 3 μm; Snider and Petters (2008)]

funded through the U.S. Bureau of Reclamation, and since its acquisition in 1977 the UWKA participated in experiments throughout the United States and in many parts of the world, funded by numerous federal and international agencies. Since 1988 the UWKA has been operated as a national facility through a cooperative agreement between the University of Wyoming and the National Science Foundation (NSF; www.eol.ucar .edu/instrumentation).
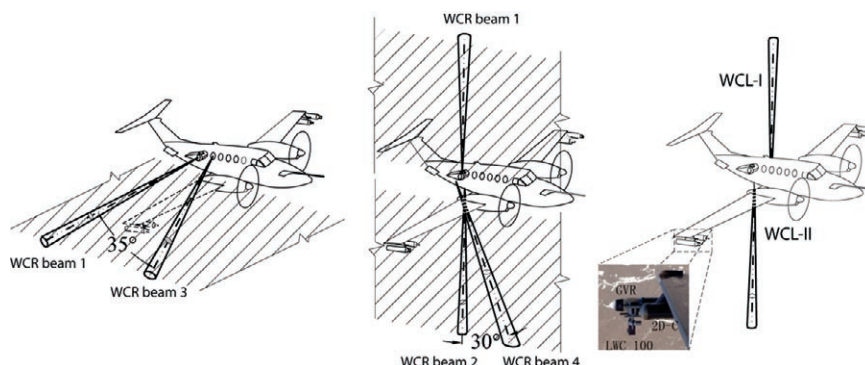

FIG. 1. A schematic of the UWKA configuration illustrating the location and looking directions for the remote sensing instruments WCR, WCL, and GVR. The inset shows one set of the wingtip-mounted pods holding the in situ cloud physics probes.

Over the last two decades there has been a concerted effort by investigators from the University of Wyoming, funded through NSF, NASA, and the Office of Naval Research, to develop a single aircraft integration of cloud radar and in situ sampling capabilities for cloud studies (Vali et al. 1995; French et al. 1999; Galloway et al. 1999). The recent addition of the Wyoming Cloud Lidar (WCL; Wang et al. 2009) led to a more complete integrated cloud observation capability on the UWKA, as part of U.S. NSF-funded Lower Atmospheric Observing Facilities (LAOF). The Wyoming Cloud Radar (WCR) and the WCL are also available for deployment on the NSF–National Center for Atmospheric Research (NCAR) C130 research aircraft. Further, the development of a 183-GHz microwave radiometer (Pazmany 2007) and its initial airborne testing on the UWKA and the NSF-C130 aircraft demonstrated the potential for an even more expanded capability. Clearly, the integration of in situ and remote sensors on a single aircraft offers important advantages from an economic and logistical point of view and allows sampling in fixed spatial relation to nonstationary meteorological features. More importantly, as illustrated by examples herein, it offers a new capability for cloud and precipitation studies.

In this paper we present analyses from the integrated remote sensing and in situ capability developed for the UWKA. In this context we present five examples from the Wyoming Airborne Integrated Cloud Observation (WAICO) experiment, a field campaign designed to explore these new capabilities. A sixth example from the Variability of the American Monsoon System (VAMOS) Ocean–Cloud–Atmosphere–Land Study (VOCALS) highlights how this capability can be used on the NSF–NCAR C130 to study different cloud systems.

INSTRUMENTATION. The UWKA team has continually developed new observational capabilities (Rodi 2011) and has most recently evolved as an airborne platform with integrated remote sensing and in situ sampling capabilities for cloud and boundary layer study. Table 1 provides a list of major cloud instrumentation available in UWKA, and Fig. 1 presents a schematic illustration of the instrument configuration.

Wyoming Cloud Radar (95 GHz). The WCR (http:// atmos.uwyo.edu/wcr) is a 95-GHz polarimetric Doppler radar utilizing a high-power klystron amplifier to provide up to 2 kW of transmit peak power. A user-controlled and programmable W-band transmit–receive electronic switching network is used to transmit and receive through up to four antennas, as illustrated in Fig. 1. The side antenna beam can be redirected to an upward-pointing beam via an external motorized reflector.

The first deployment of the WCR was in the Small Cumulus Microphysics Study (SCMS) in 1995 (French et al. 1999, 2000) and the Coastal Stratus/Marine Stratocumulus Study (CS) later that same year (Vali et al. 1998). Since that time, the WCR participated in an additional 35 studies, initially as a principal investigator (PI)-supported instrument and as part of the UWKA NSF LAOF since 2004. The WCR continually evolved since its inception as a single-antenna analog radar to today's multiantenna low-noise radar with digital receiver. The original radar was replaced with the current version of WCR in the summer of 2009. The new radar provides 10 dB better detection sensitivity and greater capability for recording more versatile pulse-pair and polarimetric parameters and full Doppler spectra. Table 2 presents the main

TABLE 2. WCR specifications.	
Transmit frequency | Wavelength	94.92 GHz | 3.16 mm
Pulse width | Pulse repetition frequency (PRF)	100–500 ns | 1–20 kHz
Antennas	Aperture | beamwidth
• Side or up (beam 1)	0.305 m | 0.7°
• Side fore (~35°, beam 3)	0.305 m | 0.7°
• Down (near nadir, beam 2)	0.457 m | 0.5°
• Down fore (~30°, beam 4)	0.381 m | 0.6°
Receiver channels	2
• Outputs	Digital (12 bits)
• Dynamic range	65 dB
• Noise figure	5 dB
Sampling rates	
• Along beam	Minimum 7.5 m
• Along flight	Minimum ~3m
Doppler radial velocity processor	
• Pulse pair	1st & 2nd moments
• Fast fourier transform (FFT) spectrum	16–512 spectral lines
Maximum unambiguous Doppler velocity	±15.8 m s^{-1} at 20 kHz PRF
Maximum measurement range	~ 10 km
First usable range gate	~ 100 m

specifications of WCR. A trihedral corner reflector is used to calibrate the up/side antenna on the ground. All other antennas are calibrated relative to that antenna from appropriate weather targets. The absolute accuracy of any of the reflectivity products is estimated to be better than 3 dB. The sensitivity of the radar varies depending on the antenna and the selected acquisition mode with values between −25 and −40 dBZ at 1 km. Real-time WCR displays are available for the operator and others onboard the aircraft.

The multibeam configurations of the WCR provide near-simultaneous measurements in horizontal and vertical planes extending from the aircraft flight path. The cross sections of radar reflectivity factor (Z_e) and Doppler velocity are used to characterize cloud and precipitation structure (Pratt et al. 2009; Wood et al. 2011a). Doppler measurements from the two sideward-pointing and the two downward-pointing antennas are used to perform dual-Doppler synthesis in a horizontal plane at the flight level and in a vertical plane along the flight track below the aircraft, rendering a high-resolution (on the order of 50×50 m^2) two-dimensional depiction of cloud and precipitation dynamics (Leon et al. 2006; Damiani and Haimov 2006). Because the WCR backscatter

signal from clouds is proportional up to the sixth power of particle size, it is dominated by the largest particles. In nonprecipitating water clouds, the WCR has enough sensitivity to detect returns from cloud droplets alone. However, in mixed-phase clouds, the WCR provides little or no information on the liquid portion of the cloud because the signal is dominated by often larger but much less numerous ice crystals.

Wyoming Cloud Lidar. The WCL is a compact polarization lidar that is used to obtain vertical profiles of backscatter and depolarization ratio. The WCL is designed to complement the WCR by providing additional cloud macrophysical and microphysical properties. For use on the UWKA, the WCL needed to be very compact, with low weight and power consumption, and utilize existing fuselage ports. The upward-pointing WCL (WCL-I) was developed in 2006 and uses a small port just forward of the door. To accommodate the small size of the receiver, a flashlamp-pumped yttrium aluminium garnet (YAG) laser operating at 355 nm is used, providing sufficient power to obtain an acceptable signal-to-noise ratio. The downward WCL (WCL-II; developed in 2007 and 2008) uses a small port near the rear of the fuselage. For this lidar, a 351-nm-wavelength diode-pumped laser was chosen to remain within the envelope of available power on the UWKA. These short wavelengths achieve eye-safe operations and provide stronger signal-to-noise ratios for molecular signals compared to lidars operating at visible or near-infrared wavelengths.

The laser head is integrated with the transmitting and receiving optics into a compact package. This compact design makes it suitable for aircraft installation and provides high mechanical stability to maintain optical alignment. The optical alignment for the short-range overlap function is designed to minimize strong short-range signals, but the receiver will still saturate under the conditions of a strong signal (Wang et al. 2009). Very recent improvements in the WCL use two detectors for the parallel or perpendicular signals, increasing the dynamic range of the instrument. The WCL relies on a high-speed analog/digital (A/D) card to provide along-beam resolutions of 3.75 m or better. Resolution along the aircraft flight track (across beam) depends on the number of shots

that must be averaged to achieve the desired signal-to-noise ratio, and typical values are 5–20 m. The WCL's first usable range gate is at about 30 m away from the aircraft. Wang et al. (2009) provide additional details about WCL-I and its measurement capabilities for clouds and aerosols.

The short operating wavelengths of the WCL allow detection of weak molecular and aerosol signals. For clouds, the WCL has considerably weaker dependence on particle size than the WCR. Therefore, in precipitating water clouds and in mixed-phase clouds, the WCL signal is often dominated by small cloud droplets. However, WCL signals can be quickly attenuated by optically thick water clouds. These characteristics of cloud signals from the WCL complement those of the WCR and offer improved cloud characterization capabilities by combining them (Wang and Sassen 2001, 2002; Wang et al. 2009).

G-band water vapor radiometer. A pod-mounted G-band water vapor radiometer (GVR) was developed by ProSensing, Inc. (Pazmany 2007). The installation on UWKA is shown in Fig. 1. The GVR measures brightness temperature using four double-sideband receiver channels, centered at 183.31 ±1, ±3, ±7, and ±14 GHz, at a rate of 24 Hz. Precipitable water vapor (PWV) and liquid water path (LWP) are estimated from the measured brightness temperatures and flight-level temperature based on a neural network trained with PWV and LWP computed from an atmospheric model generated using simulated liquid clouds combined with radiosonde data collected over a 7-yr period in Albany, New York (Pazmany 2007). Due to the high absorption rates of water vapor and liquid water near 183 GHz, the GVR has much greater sensitivity to detect LWP from aircraft or in cold regions than conventional microwave radiometers operating at 23 and 31 GHz. However, increased sensitivity comes at the cost of reduced dynamic range and at these high frequencies the receiver will saturate at lower water vapor contents leading to an inability to independently retrieve PWV and LWP in warm, high water content regions, such as the subtropics (Payne et al. 2011; Zuidema et al. 2011). PWV and LWP, combined with vertical resolved WCR and WCL measurements, are used to study the microphysical properties of mixed-phase and drizzling water clouds.

The first aircraft installation and testing of the GVR was on the National Research Council Canada (NRC) Convair 580 in 2007. Following that, the GVR was installed and tested on the UWKA for WAICO in early 2008. It was then installed on the

NSF–NCAR C130 as part of VOCALS (Zuidema et al. 2011). Since VOCALS, this tested GVR is no longer available. However, the technology to build such an instrument still exists and the examples presented in the "Observation and retrieval samples" section highlight the utility of this instrument, particularly in concert with other remote sensors.

In situ cloud probes. The UWKA is designed to be a flexible and highly configurable platform depending on the mission objectives of a given project. The UWKA facility maintains a standard suite of instruments that are capable of providing size-resolved particle distributions from ~0.1 μm to several millimeters. The UWKA carries four wingtip-mount Particle Measuring Systems, Inc. (PMS), canisters for mounting many of the standard probes for in situ cloud physics measurements. The selection of specific probes depends on the measurement requirements of the program coupled with the power, space, and weight limitations dictated by the overall instrument package. "Standard" cloud physics instruments maintained by the facility include the PMS Forward Scattering Spectrometer Probe (FSSP), and optical array probe (OAP) 2D cloud (2DC) and 2D precipitation (2DP) probes (see Table 1), all of which are relatively well-characterized instruments with known limitations (Korolev et al. 2011). Recent additions to the instrument suite include the Droplet Measurement Technologies, Inc.'s (DMT's) cloud droplet probe (CDP; Lance et al. 2010), which replaces the FSSP with a much smaller and less power-consuming package that is much less susceptible to shattering contamination of measured particle size distributions. A *fast* OAP-2DC grayscale similar to the DMT cloud imaging probe (CIP), with 64 diodes and 25-μm-resolution duplicates, significantly improves upon the measurements provided by the standard 2DC. To complement the direct particle measurements, two additional instruments—the Gerber particle volume monitor (PVM) 100A (Gerber et al. 1994) and DMT liquid water concentration (LWC) 100—provide bulk measurements of cloud liquid water content, and the Rosemount ice detector provides icing rate and an additional estimate of supercooled cloud liquid water content.

Cloud microphysical measurements may be complemented by aerosol microphysical measurements with the TSI condensation particle counter (CPC) 3025 for ultrafine nuclei and the TSI CPC 3010 for condensation nuclei (CN). Both instruments provide total aerosol concentration for particles greater than 3 and 15 nm, respectively. Size-resolved aerosol

distributions from 0.1 to about 3 μm are provided by a DMT passive cavity aerosol spectrometer probe (PCASP)-100.

In addition to facility-maintained instruments, the UWKA has extensive capability to integrate instruments belonging to outside groups. For example, a deep-cone Nevzorov probe (Korolev et al. 1998) was used to obtain redundant hotwire cloud LWC and IWC measurements in shallow, precipitating mixed-phase clouds. A closed-path laser hygrometer (CLH; Davis et al. 2007) was successfully used to retrieve total condensed water in ice clouds and mixed-phase clouds within orographic winter clouds. Probes capable of either using existing fuselage ports (for internal instruments) or existing PMS canisters are the simplest to accommodate.

As with all aircraft, the UWKA is limited by volume, weight, and power. Many additional in situ instruments that are available on larger aircraft are not available on the UWKA. For that reason, it was important to develop the remote sensing capability such that it could be transferred to other aircraft. As part of the NSF LAOF, the WCR and WCL can and have been mounted on the NSF–NCAR C130, a plane with significantly greater payload capacity and longer duration than the UWKA.

FIELD EXPERIMENTS. *WAICO experiment.* The WAICO experiment was conducted during February–March 2008 and 2009 in southeastern Wyoming. The objective of the study was to develop and demonstrate new cloud observation capabilities by first integrating remote sensors and in situ probes on the UWKA and, second, by obtaining measurements in mixed-phase clouds during late winter and early spring.

The first task is to meet the project objectives centered on installing the newly developed WCL and GVR with the WCR while maintaining a full complement of in situ probes. Successful integration of these instruments on the UWKA required novel solutions to minimize operating power requirements. During the WAICO experiments we were able to operate the WCR, WCL, and GVR with the Gerber PVM, FSSP, 2DC, and 2DP for cloud observations and the PCASP and CPC for aerosol size and concentration. Broadband radiation measurements were available from upward- and downward-looking pyranometers [Eppley precision spectral pyranometer (PSP), 0.29–2.8 μm], and pyrgeometers [Eppley precision infrared radiometer (PIR), 3.5–50 μm].

The second task was to collect data for the development and validation of combined WCR–WCL–GVR cloud retrieval algorithms. Modified versions of the ground-based multisensor algorithms created for airborne applications are required thorough validation. The WAICO flight patterns were developed and cloud targets were selected to collect proper data for this algorithm development and validation.

The third task was to collect data to study mixed-phase clouds. Compared to water- and ice-phase clouds, mixed-phase clouds are more complicated and their characteristics are less well quantified. During the WAICO experiments, we collected data from mixed-phase stratiform and wave clouds over a range of cloud temperatures and aerosol conditions.

VOCALS. VOCALS was conducted in fall 2008 off the coast of northern Chile over the northern extent of the South Pacific Ocean around 20°S latitude. VOCALS was a large, international effort to observe critical components of the coupled climate system of the South Pacific (Wood et al. 2011b). The NSF–NCAR C130 was one of five aircraft that were used to study the coupling of the chemistry, ocean, and clouds within the study area. The WCR, WCL-I, and GVR were installed on the C130 to complement the in situ measurements package for VOCALS (Zuidema et al. 2011). Cloud observations from VOCALS consisted entirely of liquid, marine stratocumulus in the subtropical boundary layer. The observations contained both precipitating (drizzle) and nonprecipitating clouds with generally low droplet concentrations. These conditions are a stark contrast to those from WAICO.

OBSERVATION AND RETRIEVAL EXAMPLES. Here we present examples from WAICO and VOCALS illustrating our new capabilities for observing clouds and for diagnosing processes occurring within them, that is, heterogeneous and homogeneous ice nucleation, drizzle, and cloud-scale dynamics. The first four examples focus on microphysics of cold clouds from WAICO. The fifth example illustrates use of a similar capability but for a marine stratocumulus cloud in VOCALS. The last example illustrates the capability of retrieving cloud dynamics properties from a WAICO case.

Wave cloud. With its relatively simple airflow structure (Heymsfield and Miloshevich 1993), wave clouds are one of the best natural targets for cloud microphysical processes study. Figure 2 presents data from a pair of wave clouds sampled during the WAICO experiment. The flight-level temperature is about −25°C. In the upwind region of the first wave (left side of Fig. 2), WCR Z_e is due to new ice formation

with a gradual increase in response to growth of the ice crystals throughout the cloud. The Z_e is continuous from the descending part of the first wave to the inflow of the second due to ice particles that survive sublimation and enter the updraft of the second wave. High attenuation and weak depolarization of the lidar signal (Figs. 2b,c) just above flight level indicate that liquid droplets were present in the rising portions of the waves. Deeper penetration of the lidar beam and high depolarization ratios reveal where in the sinking portions of the waves the water droplets evaporated and only ice was present. In those regions, the ice water content can be retrieved from the combination of WCR and WCL signals (Deng et al. 2008).

At the flight level, 2DC and FSSP measurements (Figs. 2d,e) yield size distributions of ice crystals and water droplets. The size distributions of water droplets are quite narrow because of the short growth time available in the cloud. Ice particles were detected a little later than liquid droplets in the first wave. In the second wave ice is detected right from the moment of entering the second wave. These in situ details are consistent with the WCR and WCL measurements. The broad FSSP distributions that appear in the downwind tails of the waves are artifacts resulting from shattering of large ice particles (Korolev and Isaac 2005). The PCASP (Fig. 2f) provides aerosol size distributions outside of cloud to better link cloud and aerosol microphysical properties. However, the in-cloud PCASP measurements seen here seem to be affected by the presence of ice crystals and perhaps also by the detection of partially dried hydrometeors (Strapp et al. 1992).

The in situ vertical velocity and the deduced LWP shown in Fig. 2g confirm the relatively simple dynamic structure of the waves and show that the maximum in LWP coincides, as expected, with the crest of the wave. The lower LWP maximum in the second wave is associated with the higher ice concentration there and the greater vapor uptake by these crystals via the Bergeron–Findeisen process. Although there are many potential sources of uncertainties in

GVR retrievals (Payne et al. 2011; Zuidema et al. 2011), the close-to-zero LWPs during liquid-free regions and relative variations of LWP in these wave clouds indicated that GVR LWP retrievals for these colder clouds are reliable.

Heterogeneous ice nucleation in wave clouds. Ice generation in clouds present a grand challenge to model cloud radiative impacts and precipitation formation. There are large uncertainties in parameterizing heterogeneous ice nucleation (DeMott et al. 2010). With the integrated airborne cloud observation capability, we offer new opportunities to study these phenomena.
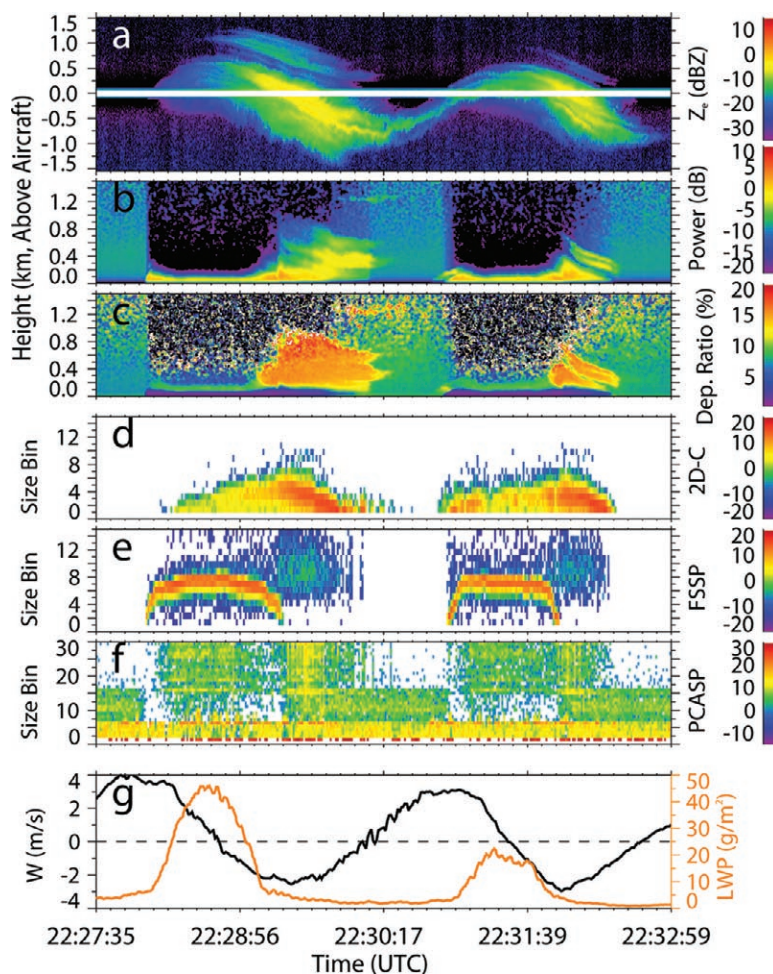

FIG. 2. A wave cloud train sampled by UWKA on 28 Feb 2008: (a) WCR radar reflectivity (the white gap indicates a zone near the aircraft without measurements), (b) WCL-I power, (c) WCL-I linear depolarization ratio (uncalibrated), (d) 2DC number concentration (*N*) for each bin [plotted as 10log(*N*)], (e) FSSP number concentration (*N*) for each bin [plotted as 10log(*N*)], (f) PCASP number concentration (*N*) for each bin [plotted as 10log(*N*)], and (g) air vertical velocity and GVR-derived LWP. The wind is blowing from left to right.
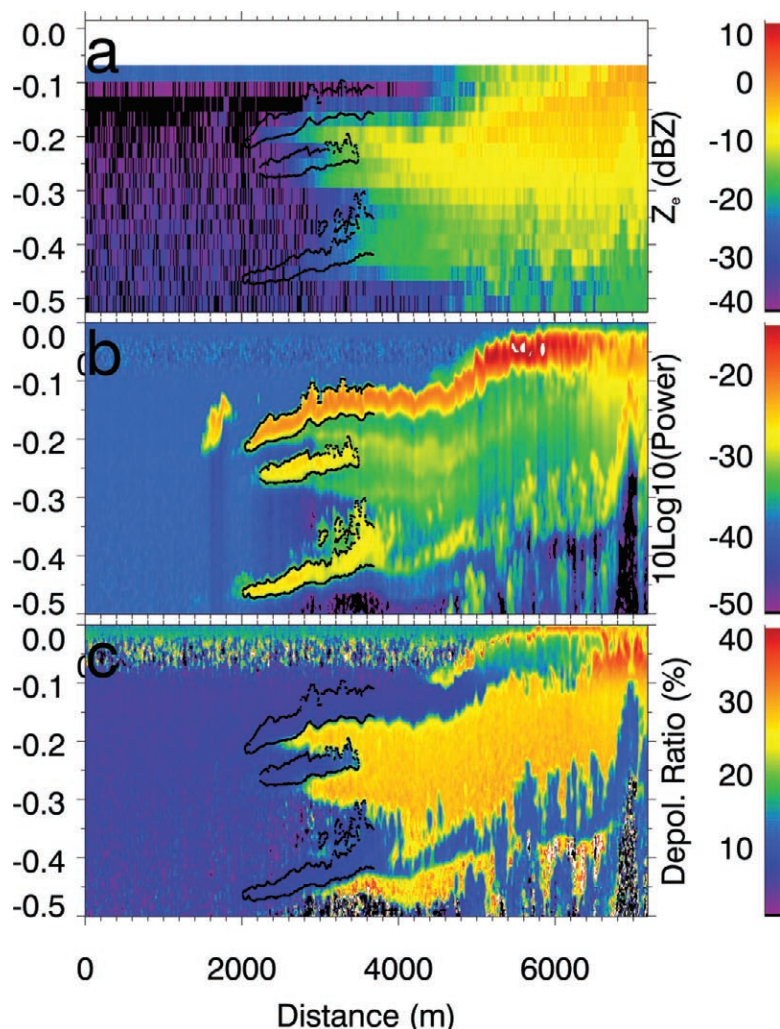
FIG. 3. WCR and WCL observations of ice formation in mixed-phase clouds on 8 Mar 2009: (a) WCR Z_e, (b) WCL-II power, and (c) WCL-II depolarization ratio (uncalibrated). The black contour outlines three distinct cloud layers; see the text for further explanation.

The rate of ice formation and its dependence on temperature in mixed-phase clouds is an especially perplexing problem. An example of its complexity and how it may be studied is illustrated in Fig. 3, showing multilayer orographically forced clouds. The black contours encompass three distinct regions of strong WCL power and low depolarization ratio outlining supercooled water-dominated mixed-phase layers, with the upwind side of the clouds on the left of figure. These three layers are separated by only 300 m and vary in temperature by only 2°C, with the uppermost layer at −31°C. The onset of WCL depolarization signal and increased WCR reflectivity provides a strong indication of the difference in location of the first onset of ice in these layers. Even with the small temperature difference between layers, ice is generated within about 200 m of the upwind edge

in the uppermost cloud and more than 500 m in the lowermost cloud. Further, the stronger depolarization signal and WCR reflectivity from the higher clouds suggests greater ice number concentration at the slightly colder temperatures. These data are consistent with a steep rise in freezing rate as a function of temperature (e.g., Vali 1994, 2008). The real-time display of such fine-scale cloud vertical structure would allow investigators to better position aircraft for detailed in situ measurements of cloud microphysical and aerosol properties.

The synergy of in situ and remote sensing sampling within wave clouds provides a more complete picture of microphysical processes in these clouds and lessens the ambiguities resulting from in situ sampling alone. Combining the velocity information from in situ and Doppler data allows the determination of parcel trajectories through wave clouds. An example is shown in Fig. 4 (top panel) of two trajectories (solid red and dashed violet lines) overlain on the WCR Z_e cross section. For each trajectory the parcels were intercepted twice by the UWKA, on the upwind (left) and downwind (right) side of the wave at the zero level indicated in the top panel. The bottom left panel (Fig. 4b) shows ice crystal spectra for both trajectories on the upwind (solid) and downwind (dashed) side of the wave. Growth to larger sizes is evident, although it must be remembered that additional ice nucleation along the trajectory is expected as the parcel undergoes further cooling (bottom right panel, dashed lines) and as crystals fall into and out of the parcel. WCR Z_e along the trajectories is consistent with the continued ice generation and growth along the trajectory and can be used to provide additional information on these processes. The observed variation of Z_e along the parcel trajectory (bottom right panel) provides further information on the evolution of the crystal population. This case demonstrates how the combined in situ and remote sensing data provide insight, confirmation of expected results, and quantitative bases for model comparisons.

Homogeneous ice nucleation.
Below approximately −35°C, pure supercooled water freezes without the aid of ice nuclei, but that simple fact is complicated by the presence of dissolved substances in high concentrations, which is the case with aerosol approaching water saturation. Although the freezing rate for homogeneous nucleation is well defined (Jeffery and Austin 1997; Pruppacher 1995) and it is generally considered to be simpler than heterogeneous ice nucleation (Cantrell and Heymsfield 2005), predicting ice number concentration generated from the homogeneous nucleation has large differences among different approaches (Lin et al. 2002; Liu and Penner 2005; Sassen and Benson 2000; Karcher and Lohmann 2003; Barahona and Nenes 2008). Field observations of homogeneous ice nucleation under different aerosol and dynamics conditions are needed to improve our capability to reliably simulate this process.

Figure 5 shows a case of homogeneous ice nucleation in a wave cloud observed on 16 March 2009. Flight-level temperature was about −41°C. In this case WCR Z_e is much weaker and increases more slowly through the cloud than in previous examples because of much smaller ice crystals. Backscatter from the WCL reveals strong attenuation throughout the cloud and the WCR
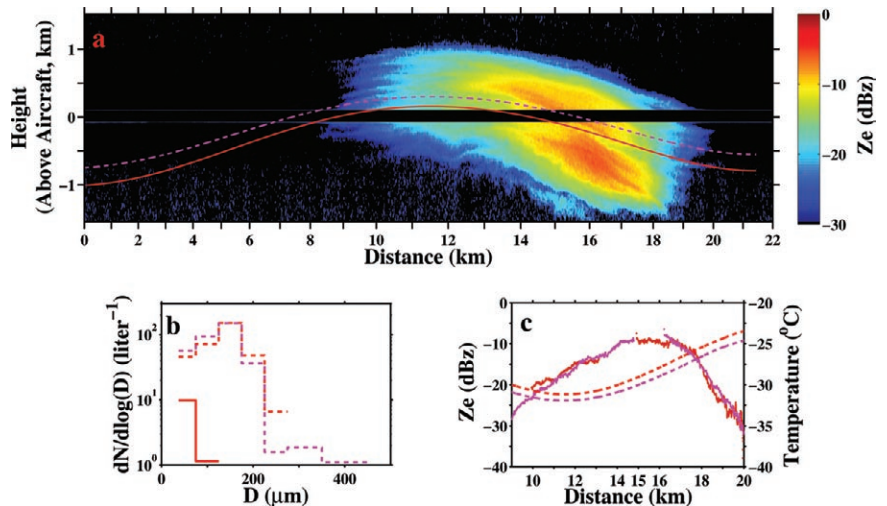

FIG. 4. Cloud and air property variations along stream lines: (a) two parcel trajectories overlaid on WCR Z_e vertical cross section, (b) ice size distributions intercepted at the flight level for the upwind (solid) and downwind (dashed) side of the cloud, and (c) air parcel temperature and Z_e along the trajectories.
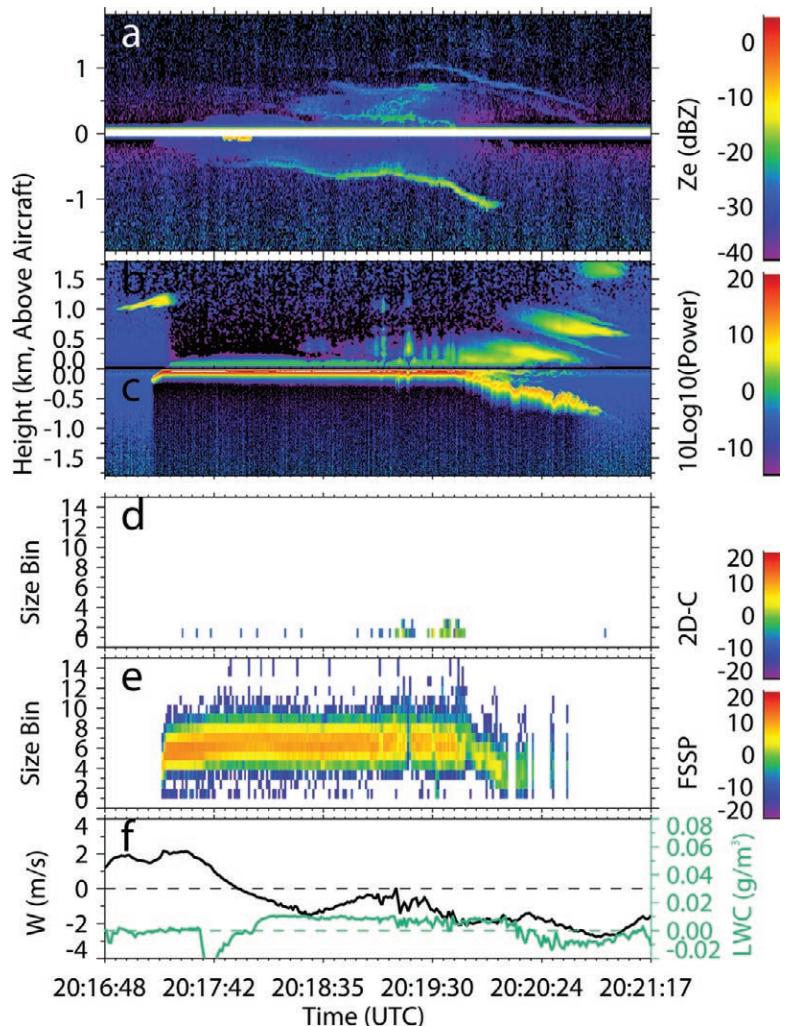
FIG. 5. A wave cloud with homogeneous ice nucleation observed on 16 Mar 2009: (a) WCR Z_e, (b),(c) up and down WCL returned power, (d) 2DC number concentration (N) [per bin in 10log(N)], (e) FSSP number concentration (N) [per bin in 10log(N)], and (f) vertical velocity (left y axis) and LWC from the hotwire probe (right y axis).

and WCL signals first appear at the same location within the cloud. These combined measurements are consistent with large numbers of very small ice crystals. The 2DC probe detected very few ice crystals. The FSSP suggests high numbers (up to 30 cm^{-3}) of small particles, but quantitative interpretation of the FSSP spectra for ice crystals is unreliable because of differences in the index of refraction of water and ice, although the total number concentration should be correct. The hotwire LWC signal is not significantly different from the clear-air noise value, confirming that very little or no liquid was present. An interesting feature of this case is the presence of narrow bands of strong WCR reflectivity. These bands occur at different temperatures and reveal some nonunderstood factors in homogeneous or heterogeneous ice nucleation in natural clouds. Further examinations of such data on homogeneous ice nucleation may open the way to improvements in its parameterization in models.

Aircraft-produced ice particles. Adiabatic expansion and the resulting cooling near the ends of propeller blades can, under the right conditions, lead to the homogeneous freezing of supercooled water in clouds. Thus, turboprop aircraft, such as the UWKA and the NSF–NCAR C130, can produce aircraft-produced ice particles (APIPs). Scientists utilizing aircraft for studies of cold processes must be cognizant of this and develop flight patterns to avoid biasing their results because of "artificially" produced ice. Woodley et al. (2003) speculate that APIPs led investigators to overestimate the development and concentrations of ice particles in clouds.

Figure 6 presents a case in which APIPs are identified from remote sensing and in situ measurements. The aircraft pass shown in the figure was along the wind (from left to right) and was preceded by another in the opposite direction by about 2 min and 150 m higher up. As seen in Fig. 6, the generally smooth Z_e structure of typical wave clouds is punctuated by patches of higher reflectivity in a pattern that is consistent with having been generated along the previous penetration. One of the high Z_e patches was sampled with the UWKA slightly after 2003 UTC. There is a significant local jump in ice concentration (2DC data) and a corresponding decrease in cloud water (FSSP data). At the same time, the CN counter shows an order of magnitude increase in aerosol concentration. These are all consistent with the generation of APIPs during the earlier pass. Clearly, such studies can lead to fuller understanding of the process of APIPs generation and of its consequences.
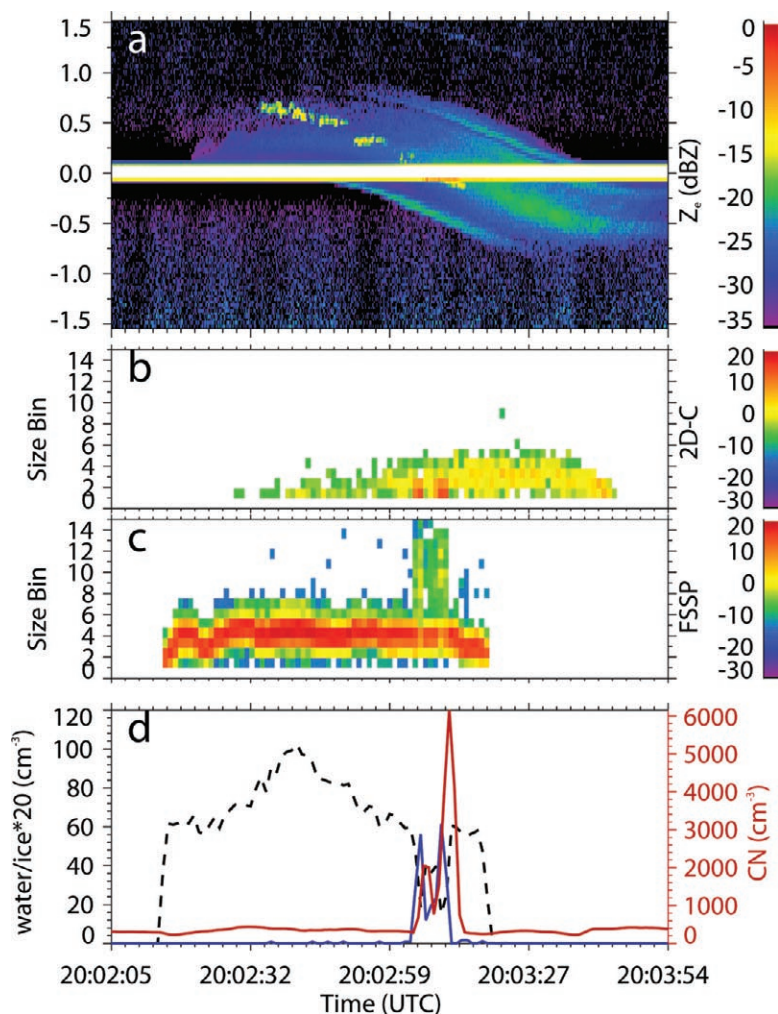
Cloud microphysical property retrievals. The synergy of multiple remote sensor airborne measurements allows for improved cloud microphysical property retrievals by using

FIG. 6. An example of APIP observed in a wave cloud on 27 Feb 2008: (a) WCR Z_e, (b) 2DC number concentration (*N*) [per bin in 10log(*N*)], (c) FSSP number concentration (*N*) [per bin in 10log(*N*)], (d) water droplet (dashed line) and ice (solid line, x20) concentration (left *y* axis) and CN concentration (right *y* axis). The flight-level temperature is ~ −25°C.

TABLE 3. A list of measurements needed to retrieve ice-, water-, and mixed-phase cloud microphysical properties.

Measurements	Ice clouds	Water clouds	Mixed-phase clouds
	IWC and D_{ge}	LWC , r_{eff} , and drizzle property	IWC and D_{ge} for ice phase LWC and r_{eff} for water phase
WCL	Extinction	Extinction	Extinction depolarization ratio
WCR	Z_e	Z_e	Z_e or spectrum
GVR		LWP	LWP
References	Donovan and van Lammeren (2001), Wang and Sassen (2002), Heymsfield et al. (2008), Deng et al. (2010)	Frisch et al. (1995), Sassen et al. (1999), O'Connor et al. (2005), Wang (2007)	Wang et al. (2004) and Shupe et al. (2008)

approaches similar to those developed for ground-based measurements. Table 3 lists the WCR, WCL, and GVR measurements needed for retrievals of water, mixed-phase, and ice cloud microphysical properties and the related published ground-based and satellite retrieval algorithms. Because ice clouds are optically thin compared with water and mixed-phase clouds, combined WCL and WCR measurements can be used to retrieve the vertical profiles of IWC and general effective radius (D_{ge}). As confirmed by Heymsfield et al. (2008), these lidar–radar approaches can yield reliable estimates of ice bulk properties. Several ground- and satellite-based approaches can be easily modified for airborne applications. Wang et al. (2009) present an example of retrievals of ice cloud microphysical properties using WCL and WCR measurements and illustrate the advantages of evaluating the retrieved parameters based on combined airborne measurements.

For stratiform water clouds without drizzle, combined WCR Z_e profiles and GVR LWP measurements are enough to provide water cloud properties (Frisch et al. 1995, 1998; Sassen et al. 1999). However, in the presence of drizzle, the drizzle drops dominate the signal from the WCR (Fig. 7a) and also contribute to LWP (Vali et al. 1995). In this
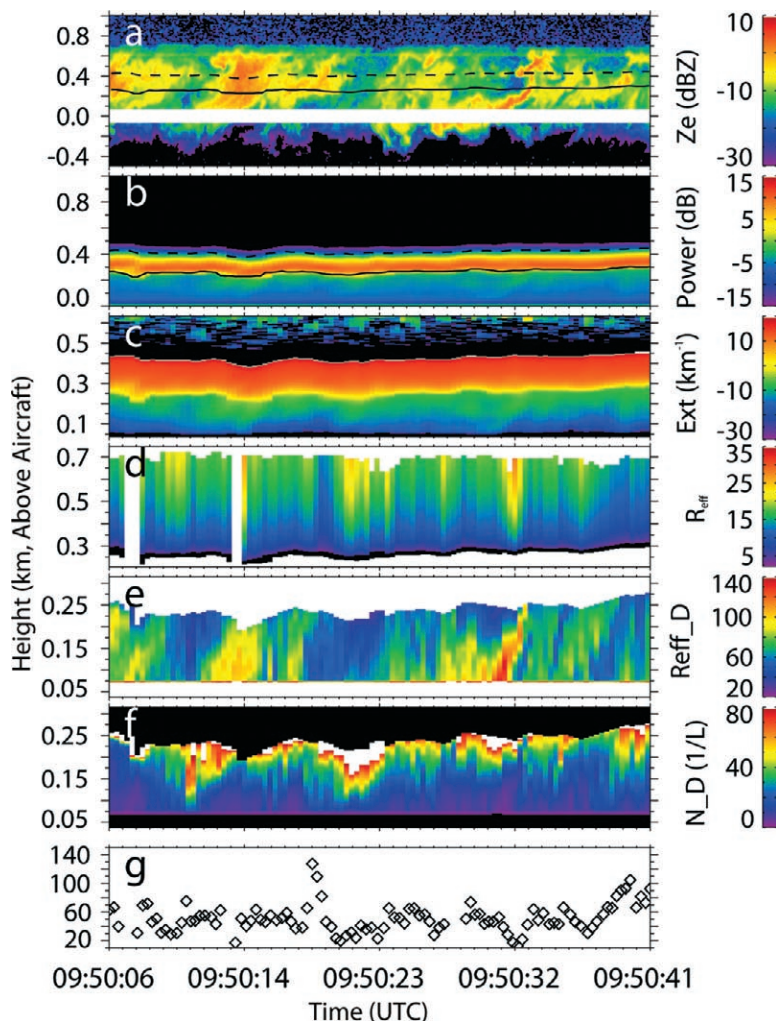

FIG. 7. WCR and WCL observations of drizzling stratocumulus clouds on 28 Oct 2008 during the VOCALS field campaign: (a) WCR Z_e, (b) WCL attenuated backscatter power, (c) retrieved visible extinction coefficient, (d) cloud effective radius (μm) above cloud base, (e) drizzle effective radius (μm) below cloud base, (f) drizzle number concentration below cloud base, and (g) layer mean cloud droplet number concentration. In (a) and (b), the WCL-identified cloud base (solid lines) and the top of useable WCL data (dashed lines) are represented.

case, we must include WCL measurements and/or additional assumptions (such as adiabatic clouds) to retrieve water droplet as well as drizzle properties. Figures 7b,c illustrate how the WCL provides strong signals for easily identifying the cloud base from using the slope change of the backscattered power and extinction (Wang and Sassen 2001). WCL signals are attenuated within about 200 m of the cloud base; estimates of cloud-top height are provided by the WCR.

Many observations have shown that adiabatic ascent of cloud parcels is a reasonable assumption for most stratiform warm clouds, especially at small spatial scales and within the lower parts of clouds (Albrecht et al. 1990; Zuidema et al. 2005; Korolev et al. 2007), although some uncertainty remains because of our inability to accurately measure temperature within cloud (Heymsfield et al. 1979). With in situ measurements obtained not far below the cloud base, the cloud-base temperature can be reliably estimated and used to estimate an adiabatic LWC profile within about 300 m above the cloud base. With the assumption of lognormal size distribution of constant width, the lidar-derived cloud extinction profiles were combined with LWC profiles to derive mean cloud number concentration and effective radius profiles (Frisch et al. 1995); the retrieved r_{eff} profiles and mean droplet concentration are presented in Figs. 7d,g. Drizzle properties were derived from the WCR and WCL measurements below the cloud base (O'Connor et al. 2005); the retrieved drizzle effective radius and total concentration are presented in Figs. 7e,f.

Stratiform mixed-phase clouds and drizzling stratocumulus have similar vertical structures (Wang et al. 2004). A combination of WCL and GVR measurements of LWP can be used to characterize supercooled water cloud properties. Combining WCR and WCL below the mixed-phase layer can be used to derive ice-phase properties.

Cloud dynamics retrievals. The dual-Doppler capability of the WCR provides a unique tool for the study of interactions between cloud-scale dynamics and cloud microphysics. WCR dual-Doppler measurements have been used to investigate cloud-scale dynamics in marine stratocumulus (Leon et al. 2006) and in much more vigorous cumulus congestus (Damiani et al. 2006). Figure 8 presents a similar analysis (Damiani and Haimov 2006) of an orographically forced convective cloud. Although WCL-II signals are quickly attenuated by supercooled water on the upwind side (right), the lidar data show the upper-cloud boundary and glaciation in the downwind side (left) well. The WCR measurements show details of the spatial variation of Z_e throughout the depth of the cloud. Dual-Doppler retrievals of 2D winds (Figs. 8c,d; 15 m s^{-1} mean horizontal wind is removed from the plot) reveal dominant upward motion on the upwind side and complex circulations on the downwind side. By overlaying the wind vectors on Z_e (contributed mostly by ice crystals),
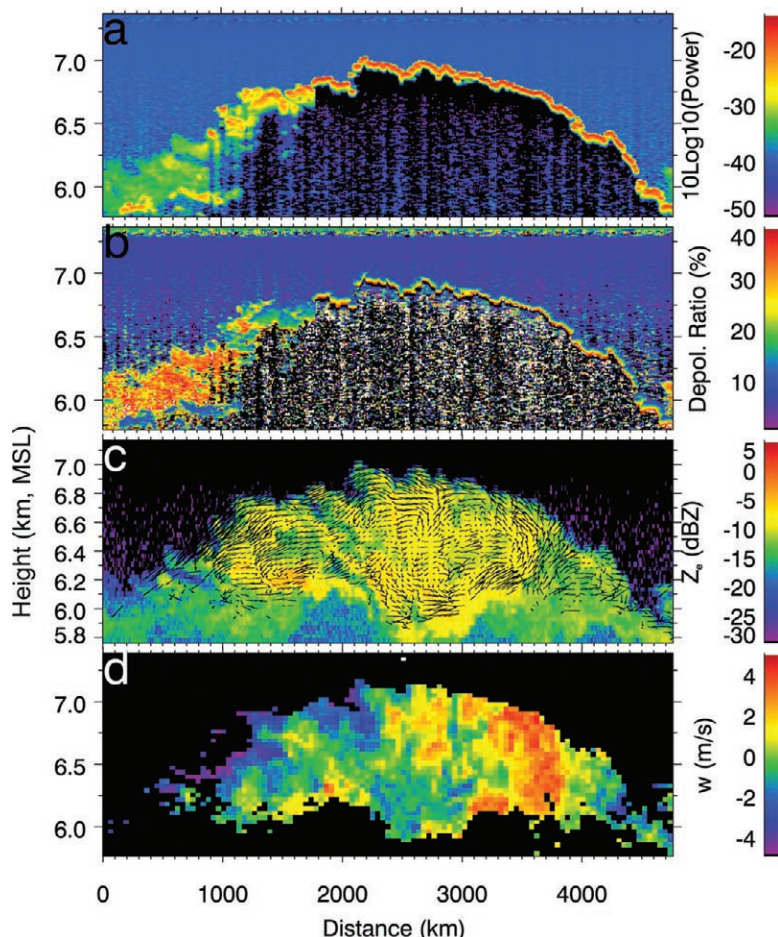

FIG. 8. WCL (a) backscattered power and (b) depolarization ratio from an orographically induced convective cloud. Resultant wind vectors (mean wind has been removed) retrieved from a dual-Doppler synthesis and overlain on the (c) WCR Z_e field and (d) retrieved vertical wind velocity for the same convective cloud.

the relationship between the cloud-scale dynamics and precipitation development is depicted.

SUMMARY. The examples presented here demonstrate successful integration of the WCR, WCL, GVR, and the in situ cloud physics and aerosol probes on the UWKA and their use on other aircraft, the NSF–NCAR C130. Combined analyses of the multiple remote sensor and detailed microphysical measurements lead to better insights of key processes within clouds. We have shown that the remote sensing measurements provide important context for interpretation of the microphysics measurements and extend microphysics measurements away from the aircraft and along trajectories for interpreting the evolution of hydrometeors within clouds. Because the different remote sensors have different sensitivities to particles of different sizes, shapes, and phases, the radar–lidar–radiometer package provides better diagnoses of physical processes occurring in clouds than can be determined through in situ measurements alone or with just one of these remote sensors.

Algorithm development and validation for cloud macrophysical properties continues. Cases presented here highlight present capabilities for warm and cold clouds. Algorithms developed for ground-based and/or satellite-based schemes can be adopted to the airborne instrument suite and the addition of in situ measurements provides additional constraints for refinements of these algorithms for a variety of conditions.

Since the first WAICO campaign in the winter of 2008, the integrated cloud remote sensing platform has been used in six field campaigns, ranging from winter orographically forced clouds in the intemountain west to summer deep tropical convection. The WCR and both WCLs, supported through the NSF-funded LAOF, have been migrated to and are also available on the NSF–NCAR C130. That platform provides opportunities for other flight missions and has the capacity for significantly more and a broader range of in situ measurements. In the meantime, further development continues on the UWKA. With new instruments that are smaller and require less power, the UWKA continues to improve its in situ cloud microphysics measurements. Expansions of the real-time data display capabilities will allow scientists to utilize more information in making decisions on how best to position the aircraft and optimize the observations.

REFERENCES

Albrecht, B. A., C. Fairall, D. Thomson, A. White, and J. Snider, 1990: Surface-based remote sensing of the observed and the adiabatic liquid water content. *Geophys. Res. Lett.,* **17,** 89–92.

Bailey, M. P., and J. Hallett, 2009: A comprehensive habit diagram for atmospheric ice crystals: Confirmation from the laboratory, AIRS II, and other field studies. *J. Atmos. Sci.,* **66,** 2888–2899.

Baker, B. A., and R. P. Lawson, 2006: In situ observations of the microphysical properties of wave, cirrus, and anvil clouds. Part I: Wave clouds. *J. Atmos. Sci.,* **63,** 3160–3185.

Barahona, D., and A. Nenes, 2008: Parameterization of cirrus cloud formation in large-scale models: Homogeneous nucleation. *J. Geophys. Res.,* **113,** D11211, doi:10.1029/2007JD009355.

Cantrell, W., and A. J. Heymsfield, 2005: Production of ice in tropospheric clouds: A review. *Bull. Amer. Meteor. Soc.,* **86,** 795–807.

Damiani, R., and S. Haimov, 2006: A high resolution dual-Doppler technique for fixed multiantenna airborne radar. *IEEE Trans. Geosci. Remote Sens.,* **44,** 3475–3489.

——, G. Vali, and S. Haimov, 2006: The structure of thermals in cumulus from airborne dual-Doppler radar observations. *J. Atmos. Sci.,* **63,** 1432–1450.

Davis, S., A. G. Hallar, and L. Avallone, 2007: Measurement of total water with a tunable diode laser hygrometer: Inlet analysis, calibration procedure, and ice water content determination. *J. Atmos. Oceanic Technol.,* **24,** 463–475.

DeMott, P. J., and Coauthors, 2010: Predicting global atmospheric ice nuclei distributions and their impacts on climate. *Proc. Natl. Acad. Sci. USA,* **107,** 11 217–11 222, doi:10.1073/pnas.0910818107.

Deng, M., Z. Wang, G. Vali, S. Haimov, and J. French, 2008: Wave cloud properties observed from Wyoming cloud lidar and radar during the ICE-L field campaign. *Proc. 24th Int. Laser Radar Conf.,* Boulder, CO, International Coordination Group on Laser Atmospheric Studies (ICLAS), 917–920.

——, G. G. Mace, Z. Wang, and H. Okamoto, 2010: Tropical Composition, Cloud and Climate

Coupling Experiment validation for cirrus cloud profiling retrieval using CloudSat radar and CALIPSO lidar. *J. Geophys. Res.,* **115,** D00J15, doi:10.1029/2009JD013104.

Donovan, D. P., and A. C. A. P. van Lammeren, 2001: Cloud effective particle size and water content profile retrievals using combined lidar and radar observations—1. Theory and examples. *J. Geophys. Res.,* **106,** 27 425–27 448.

French, J., G. Vali, and R. D. Kelly, 1999: Evolution of small cumulus clouds in Florida: Observations of pulsating growth. *Atmos. Res.,* **52,** 143–165.

——, ——, and ——, 2000: Observations of microphysics pertaining to the development of drizzle in warm, shallow cumulus clouds. *Quart. J. Roy. Meteor. Soc.,* **126,** 415–443.

Fritsch, J. M., and R. E. Carbone, 2004: Improving quantitative precipitation forecasts in the warm season: A USWRP research and development strategy. *Bull. Amer. Meteor. Soc.,* **85,** 955–965.

——, C. W. Fairall, and J. B. Snider, 1995: Measurement of stratus cloud and drizzle parameters in ASTEX with a K_e-band Doppler radar and a microwave radiometer. *J. Atmos. Sci.,* **52,** 2788–2799.

——, G. Feingold, C. W. Fairall, T. Uttal, and J. B. Snider, 1998: On cloud radar and microwave radiometer measurements of stratus cloud liquid water profiles. *J. Geophys. Res.,* **103,** 23 195–23 197.

Galloway, J., and Coauthors, 1999: Coincident in situ and W-band radar measurements of drop size distribution in a marine stratus cloud and drizzle. *J. Atmos. Oceanic Technol.,* **16,** 504–517.

Gerber, H., B. G. Arends, and A. S. Ackerman, 1994: New microphysics sensor for aircraft use. *Atmos. Res.,* **31,** 235–252.

Gordon, G. L., and J. D. Marwitz, 1984: An airborne comparison of three PMS probes. *J. Atmos. Oceanic Technol.,* **1,** 22–27.

Heymsfield, A. J., and L. M. Miloshevich, 1993: Homogeneous ice nucleation and supercooled liquid water in orographic wave clouds. *J. Atmos. Sci.,* **50,** 2235–2353.

——, J. E. Dye, and C. J. Biter, 1979: Overestimates of entrainment from wetting of aircraft temperature sensors in cloud. *J. Appl. Meteor.,* **18,** 92–95.

——, and Coauthors, 2008: Testing IWC retrieval methods using radar and ancillary measurements with in situ data. *J. Appl. Meteor. Climatol.,* **47,** 135–163.

Heymsfield, G. M., and Coauthors, 1996: The EDOP radar system on the high-altitude NASA ER-2 aircraft. *J. Atmos. Oceanic Technol.,* **13,** 795–809.

Hildebrand, P. H., and Coauthors, 1996: The ELDORA/ ASTRAIA airborne Doppler weather radar: High-

resolution observations from TOGA COARE. *Bull. Amer. Meteor. Soc.,* **77,** 213–232.

Isaac, G. A., and K. S. Schmidt, 2009: Cloud properties from in-situ and remote sensing measurements, capability and limitations. *Clouds in the Perturbed Climate System,* J. Heintzenberg and R. J. Charlson, Eds., The MIT Press, 73–106.

Jeffery, C., and P. Austin, 1997: Homogeneous nucleation of supercooled water: Results from a new equation of state. *J. Geophys. Res.,* **102,** 25 269–25 279.

Karcher, B., and U. Lohmann, 2003: A parameterization of cirrus cloud formation: Heterogeneous freezing. *J. Geophys. Res.,* **108,** 4402, doi:10.1029 /2002JD003220.

Klein, S. A., and Coauthors, 2009: Intercomparison of model simulations of mixed phase clouds observed during the ARM Mixed-Phase Arctic Cloud Experiment. Part I: Single-layer cloud. *Quart. J. Roy. Meteor. Soc.,* **135,** 979–1002, doi:10.1002/qj.416.

Korolev, A. V., and G. A. Isaac, 2005: Shattering during sampling by OAPS and HVPS. Part I: Snow particles. *J. Atmos. Oceanic Technol.,* **22,** 528–542.

——, J. W. Strapp, G. A. Isaac, and A. N. Nevzorov, 1998: The Nevzorov airborne hot-wire LWC–TWC probe: Principle of operation and performance characteristics. *J. Atmos. Oceanic Technol.,* **15,** 1495–1510.

——, G. A. Isaac, J. W. Strapp, S. G. Cober, and H. W. Barker, 2007: In situ measurements of liquid water content profiles in midlatitude stratiform clouds. *Quart. J. Roy. Meteor. Soc.,* **133,** 1693–1699.

——, E. F. Emery, J. W. Strapp, S. G. Cober, G. A. Isaac, M. Wasey, and D. Marcotte, 2011: Small ice particles in tropospheric clouds: Fact or artifact? Airborne Icing Instrumentation Evaluation Experiment. *Bull. Amer. Meteor. Soc.,* **92,** 967–973.

Lance, S., C. A. Brock, D. Rogers, and J. A. Gordon, 2010: Water droplet calibation of the cloud droplet probe and in-flight performance in liquid, ice and mixed-phase clouds during ARCPAC. *Atmos. Meas. Tech.,* **3,** 1683–1706.

Leon, D., G. Vali, and M. Lothon, 2006: Dual-Doppler analysis in a single plane from an airborne platform. Part I: Technique. *J. Atmos. Oceanic Technol.,* **23,** 3–21.

Lin, R., D. Starr, P. J. DeMott, R. Cotton, K. Sassen, E. J. Jensen, B. Kärcher, and X. Liu, 2002: Cirrus parcel model comparison project. Phase I: The critical components to simulate cirrus initiation explicitly. *J. Atmos. Sci.,* **59,** 2305–2328.

Liu, X., and J. E. Penner, 2005: Ice nucleation parameterization for global models. *Meteor. Z.,* **14,** 499–514.

McFarquhar, G. M., G. Zhang, M. R. Poellot, G. L. Kok, R. McCoy, T. Tooman, A. Fridlind, and A. J. Heymsfield, 2007: Ice properties of single-layer stratocumulus during the Mixed-Phase Arctic Cloud Experiment: 1. Observations. *J. Geophys. Res.,* **112,** D24201, doi:10.1029/2007JD008633.

McGill, M. J., D. L. Hlavka, W. D. Hart, J. D. Spinhirne, V. S. Scott, and B. Schmid, 2002: The cloud physics lidar: Instrument description and initial measurement results. *Appl. Opt.,* **41,** 3725–3734.

NRC, 1998: *The Atmospheric Sciences Entering the Twenty-First Century.* National Academy Press, 384 pp.

O'Connor, E. J., R. J. Hogan, and A. J. Illingworth, 2005: Retrieving stratocumulus drizzle parameters using Doppler radar and lidar. *J. Appl. Meteor.,* **44,** 14–27.

Payne, V. H., E. J. Mlawer, K. E. Cady-Pereira, and J. Moncet, 2011: Water vapor continuum absorption in the microwave. *IEEE Trans. Geosci. Remote Sens.,* **49,** 2194–2208.

Pazmany, A. L., 2007: A compact 183-GHz radiometer for water vapor and liquid water sensing. *IEEE Trans. Geosci. Remote Sens.,* **45,** 2202–2206.

Pratt, K. A., and Coauthors, 2009: In situ detection of biological particles in cloud ice-crystals. *Nat. Geosci.,* **2,** 398–401, doi:10.1038/ngeo521.

Pruppacher, H., 1995: A new look at homogeneous ice nucleation in supercooled water drops. *J. Atmos. Sci.,* **52,** 1924–1933.

Randall, D., M. Khairoutdinov, A. Arakawa, and W. Grabowski, 2003: Breaking the cloud parameterization deadlock. *Bull. Amer. Meteor. Soc.,* **84,** 1547–1564.

Rangno, A. L., and P. V. Hobbs, 1991: Ice particle concentrations and precipitation development in small polar maritime cumuliform clouds. *Quart. J. Roy. Meteor. Soc.,* **117,** 207–241.

——, and ——, 2001: Ice particles in stratiform clouds in the arctic and possible mechanisms for the production of high ice concentrations. *J. Geophys. Res.,* **106,** 15 065–15 075.

Rodi, A., 2011: King of the air: The evolution and capabilities of Wyoming's observation aircraft. *Meteorological Technology International,* May 2011, UKIP, 44–47.

Sassen, K., and S. Benson, 2000: Ice nucleation in cirrus clouds: A model study of the homogeneous and heterogeneous modes. *Geophys. Res. Lett.,* **27,** 521–524.

——, G. G. Mace, Z. Wang, S. M. Sekelsky, and R. E. McIntosh, 1999: Continental stratus clouds: A case study using coordinated remote sensing and aircraft measurements. *J. Atmos. Sci.,* **56,** 2345–2358.

Shupe, M. D., and Coauthors, 2008: A focus on mixed-phase clouds: The status of ground-based observational methods. *Bull. Amer. Meteor. Soc.,* **89,** 1549–1562.

Snider, J. R., and M. D. Petters, 2008: Optical particle counter measurement of marine aerosol hygroscopic growth. *Atmos. Chem. Phys.,* **8,** 1949–1962.

Soden, B. J., and I. M. Held, 2006: An assessment of climate feedbacks in coupled ocean–atmosphere models. *J. Climate,* **19,** 3354–3360.

Solomon, S., D. Qin, M. Manning, Z. Chen, M. Marquis, K. B. Averyt, M. Tignor, and H. L. Miller, Eds., 2007: *Climate Change 2007: The Physical Science Basis.* Cambridge University Press, 996 pp.

Stephens, G. L., and Coauthors, 2002: The CloudSat mission and the A-Train: A new dimension to space-based observations of clouds and precipitation. *Bull. Amer. Meteor. Soc.,* **83,** 1771–1790.

Stevens, B., and Coauthors, 2003: Dynamics and Chemistry of Marine Stratocumulus—DYCOMS-II. *Bull. Amer. Meteor. Soc.,* **84,** 579–593.

Stoelinga, M. T., and Coauthors, 2003: Improvement of microphysical parameterization through observational verification experiment. *Bull. Amer. Meteor. Soc.,* **84,** 1807–1826.

Strapp, J. W., W. R. Leaitch, and P. S. K. Liu, 1992: Hydrated and dried aerosol-size-distribution measurements from Particle Measuring Systems FSSP-300 probe and deiced PCASP-100x probe. *J. Atmos. Oceanic Technol.,* **9,** 548–555.

Vali, G., 1994: Freezing rate due to heterogeneous nucleation. *J. Atmos. Sci.,* **51,** 1843–1856.

——, 2008: Repeatability and randomness in heterogeneous freezing nucleation. *Atmos. Chem. Phys.,* **8,** 5017–5031.

——, R. D. Kelly, A. Pazmany, and R. E. McIntosh, 1995: Airborne radar and in-situ observations of a shallow stratus with drizzle. *Atmos. Res.,* **38,** 361–380.

——, ——, J. French, S. Haimov, D. Leon, R. McIntosh, and A. Pazmany, 1998: Finescale structure and microphysics of coastal stratus. *J. Atmos. Sci.,* **55,** 3540–3563.

Wang, Z., 2007: A refined two-channel microwave radiometer liquid water path retrieval for cold regions by using multiple-sensor measurements. *IEEE Geosci. Remote Sens. Lett.,* **4,** 591–595.

——, and K. Sassen, 2001: Cloud type and macrophysical property retrieval using multiple remote sensors. *J. Appl. Meteor.,* **40,** 1665–1682.

——, and ——, 2002: Cirrus cloud microphysical property retrieval using lidar and radar measurements. Part I: Algorithm description and comparison with in situ data. *J. Appl. Meteor.,* **41,** 218–229.

——, ——, D. Whiteman, and B. Demoz, 2004: Studying altocumulus plus virga with ground-based active and passive remote sensors. *J. Appl. Meteor.,* **43,** 449–460.

——, G. M. Heymsfield, L. Li, and A. J. Heymsfield, 2005: Retrieving optically thick ice cloud microphysical properties by using airborne dual-wavelength radar measurements. *J. Geophys. Res.,* **110,** D19201, doi:10.1029/2005JD005969.

——, P. Wechsler, W. Kuestner, J. French, A. Rodi, B. Glover, M. Burkhart, and D. Lukens, 2009: Wyoming cloud lidar: Instrument description and applications. *Opt. Express,* **17,** 13 576–13 587.

Wood, R., C. S. Bretherton, D. Leon, A. D. Clarke, P. Zuidema, G. Allen, and H. Coe, 2011a: An aircraft case study of the spatial transition from closed to open mesoscale cellular convection. *Atmos. Chem. Phys.,* **11,** 2341–2370.

——, and Coauthors, 2011b: The VAMOS Ocean-Cloud-Atmosphere-Land Study Regional Experiment (VOCALS-REx): Goals, platforms, and field operations. *Atmos. Chem. Phys.,* **11,** 628–654, doi:10.5194/acp-11-627-2011.

Woodley, W. L., G. Gordon, T. J. Hendereson, B. Vonnegut, D. Rosenfeld, and A. Detwiler, 2003: Aircraft-produced ice particles (APIPS): Additional results and further insights. *J. Appl. Meteor.,* **42,** 640–651.

Zuidema, P., E. R. Westwater, C. Fairall, and D. Hazen, 2005: Ship-based liquid water path estimates in marine stratocumulus. *J. Geophys. Res.,* **110,** D20206, doi:10.1029/2005JD005833.

——, D. Leon, A. Pazmany, and M. Cadeddu, 2011: Aircraft millimeter-wave retrievals of cloud liquid water path during VOCALS-REx. *Atmos. Chem. Phys. Discuss.,* **11,** 19 581–19 616, doi:10.5194/acpd-11-19581-2011.